Bioinsp. Biomim. **5** (2010) 035003 (14pp) doi:10.1088/1748-3182/5/3/035003

A biorobotic model of the sunfish pectoral fin for investigations of fin sensorimotor control

Chris Phelan[1], **James Tangorra**[1,4], **George Lauder**[2] **and Melina Hale**[3]

[1] Department of Mechanical Engineering, Drexel University, Philadelphia, PA 19104, USA
[2] Museum of Comparative Zoology, Harvard University, Cambridge, MA 02138, USA
[3] Department of Organismal Biology and Anatomy, University of Chicago, Chicago, IL 60637, USA

E-mail: tangorra@coe.drexel.edu

Received 24 May 2010
Accepted for publication 28 July 2010
Published 20 August 2010
Online at stacks.iop.org/BB/5/035003

Abstract
A comprehensive understanding of the control of flexible fins is fundamental to engineering underwater vehicles that perform like fish, since it is the fins that produce forces which control the fish's motion. However, little is known about the fin's sensory system or about how fish use sensory information to modulate the fin and to control propulsive forces. As part of a research program that involves neuromechanical and behavioral studies of the sunfish pectoral fin, a biorobotic model of the pectoral fin and of the fin's sensorimotor system was developed and used to investigate relationships between sensory information, fin ray motions and propulsive forces. This robotic fin is able to generate the motions and forces of the biological fin during steady swimming and turn maneuvers, and is instrumented with a relatively small set of sensors that represent the biological lateral line and receptors hypothesized to exist intrinsic to the pectoral fin. Results support the idea that fin ray curvature, and the pressure in the flow along the wall that represents the fish body, capture time-varying characteristics of the magnitude and direction of the force created throughout a fin beat. However, none of the sensor modalities alone are sufficient to predict the propulsive force. Knowledge of the time-varying force vector with sufficient detail for the closed-loop control of fin ray motion will result from the integration of characteristics of many sensor modalities.

(Some figures in this article are in colour only in the electronic version)

1. Introduction

A biorobotic model of the bluegill sunfish (*Lepomis macrochirus*) pectoral fin and pectoral fin sensorimotor system (figure 1) has been developed as an experimental tool for investigations of fin sensorimotor control in fishes. A comprehensive understanding of the control of flexible fins is fundamental to engineering underwater vehicles that perform in a manner on par with fish since it is the fins that produce the forces which control the fish's motion. However, little is known about the sensory apparatus of pectoral fins, the neural mechanisms involved in fin control, or how mechanical and hydrodynamic information about the fin and flow is used to modulate the motions and physical properties of the fin. These issues are being studied via a research program that integrates biorobotic modeling with behavioral studies of the sunfish pectoral fin and neurobiological studies of the fin's sensorimotor system. The biorobotic system consists of a fin-rayed pectoral fin that can reproduce the motions and propulsive forces of the biological fin, sensors that model the sensory systems extrinsic and intrinsic to the fin, and a real-time, programmable control system that can execute traditional and biologically derived control strategies. The biorobotic fin is being used to implement what is learned from the behavioral and neurobiological studies, and in turn, to stimulate questions from a control systems and information processing perspective

[4] Author to whom any correspondence should be addressed.

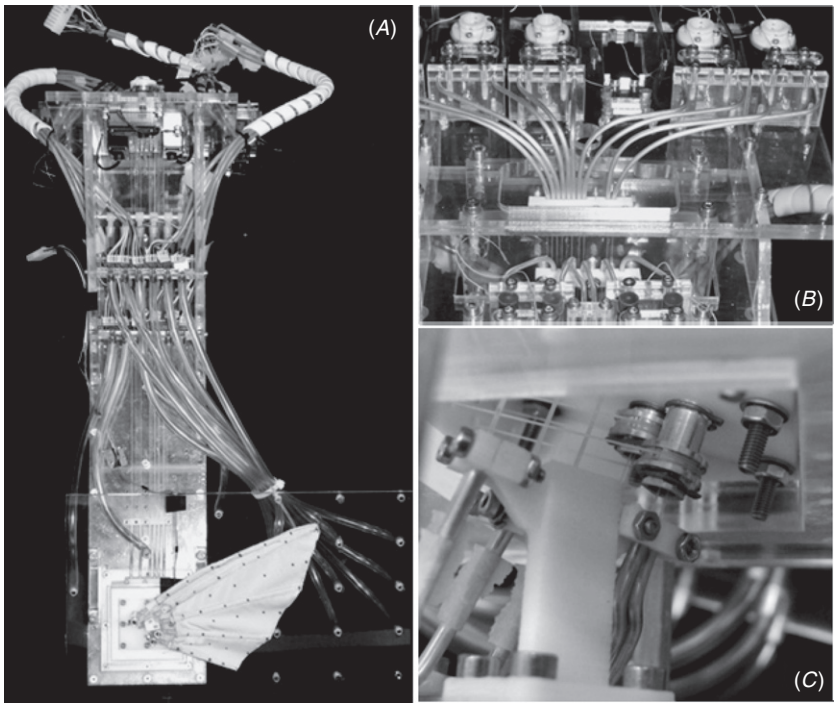

Figure 1. Biorobotic fin system. Lateral view showing the fin (with black markers which allow video tracking of fin kinematics), the flat plate with pressure ports behind the fin and the supporting framework to guide tendons to the fin ray base (*A*). Top of system (*B*) showing servomotors and mandrel bent tubing that guide tendons to the fin rays (*B*). Back of fin base (*C*) showing rotational axes driven by tendons. The mechanism provides 2 degrees of freedom, and decouples the sweep of the fin ray from the rotary motions.

that will be answered through additional behavioral and neurobiological experimentation.

The physical mechanisms that contribute to the production of propulsive forces by highly flexible fins are well understood and are reasonably straightforward to model with a biorobotic fin (Tangorra *et al* 2009, 2010, Gottlieb *et al* 2010). Propulsive forces are created through an exchange of energy between the fin and the water. As the pectoral fin moves, vortices develop along the fin's edges, the fin bends and stores energy elastically, and the vortices are shed into the flow along with jets (Mittal *et al* 2006, Dong *et al* 2010). The complex motions which cause this exchange of energy are the result of driven motions at the fin ray roots and a dynamic interaction between the flexible fin and the water. Forces are therefore modulated through changes to movement patterns and active adjustments of the fin's mechanical properties (Colgate and Lynch 2004, Tangorra *et al* 2010). These changes may be subtle, such as when the fin is stiffened as swimming speed increases, or the changes may be obvious, such as when the fin gait shifts to execute a maneuver (Gottlieb *et al* 2010).

In contrast to the biomechanics of pectoral fin swimming, little is known about the sensory organization intrinsic to the fin, or of the relationship between extrinsic sensory inputs (e.g., vision and lateral line (Coombs and Van Netten 2006)) and the motor outputs that drive the fin rays. This introduces significant uncertainty into the design of a model sensory system, the integration of sensory information and the development of biologically derived control strategies. The fine level of control that the sunfish has over pectoral fin motions and mechanical properties suggests that there is closed-loop, sensory-based control of the fin. The ability of an animal to adjust movement patterns to maintain locomotion is due to sensory input that—through altering firing patterns of active neurons or recruiting new neurons—is used to fine tune motor output. It is clear that this occurs in sunfish, as stroke-by-stroke differences in pectoral fin behaviors and motor patterns are typical. Although sensory systems in terrestrial vertebrates are well understood, it is unclear if similar joint and muscle sensors are present in pectoral fin muscle groups in fishes. There is only a single (questionable) report of muscle spindles in fish, and that is in the jaw muscle of salmon (Maeda *et al* 1983). The nervous system in fishes is believed to sense muscle dynamics with free sensory nerve endings (Ono 1982), although physiological demonstrations of such proprioceptive inputs from locomotor muscle are non-existent. The types and distribution of the sensory components associated with the fin rays and the fin membrane are also unknown. Labeling of nerves in zebrafish has demonstrated that there is an array of sensory fibers associated with each fin ray and the leading edge of the fin (Thorsen and Hale 2007), and it is possible that the fishes sense pressure, touch or the bending of the fin ray and membrane via these nerves.

In this paper we will (1) discuss functional requirements for the biorobotic fin and fin sensorimotor system; (2) present the design of a new generation biorobotic fin system that contains sensory receptors for fluid pressure and strain and (3) present results from experimental trials conducted to help understand relationships between the sensory information available to the fin, the motions of the fin rays and the propulsive forces created by the fin. In particular, three

hypotheses were considered. First, there is a significant lag between the driven movements of the fin rays and the resultant forces produced by the highly deformable pectoral fin. This lag was expected to be dependent on fin ray stiffness and could make it difficult to control the instantaneous motions of fin rays effectively based solely on sensory measures (e.g., vestibular and visual) of the motions of the fish caused by fin forces. Second, flow pressure downstream of the fin correlates with the 2D propulsive force, where the 2D propulsive force is the vectorial combination of the measured thrust and lateral forces, and with the frequency of the fin beat. Third, the bending of the fin correlates with the direction of the 2D propulsive force, and not with the magnitude of the force. Since the stiffness of the fin rays can be actively modulated by the fish (Alben *et al* 2007), the relationship between fin bending and fin forces is not invariant. The curvature of the fin rays does, however, dictate the shape of the fin, and therefore the direction of the propulsive force. The outcome of this preliminary investigation was a clearer understanding of how the fin may 'feel' its interaction with the water. This is a first step toward learning what information from the multiple sensory modalities is relevant to the control of fin motions and the production of useful force.

2. System design

The governing objective was to develop a biorobotic system that was an effective experimental tool for investigations of closed-loop sensorimotor control of the fin. To achieve this, the system must produce and sense the physical and fluidic phenomena that are relevant to the control of the biological fin, and have a physical and computational architecture that allows for sensory, learning and control strategies to be explored. Based on these functional requirements, the system's architecture was defined to include a flexible, fin-rayed pectoral fin, a suite of sensors, and a scalable controller capable of data acquisition (DAQ), signal processing, control computation, and providing motor control outputs.

2.1. Biorobotic fin

2.1.1. Functional requirements. The biorobotic fin has to produce motions, forces and flows similar to those of the biological fin, and must have the ability to adjust the motions and properties of individual fin rays. This renders the appropriate mechanical and hydrodynamic information available for the closed-loop control of the fin and makes it possible for the fin to respond to changes in sensory information and to higher level supervisory commands. Initially, a single fin that can execute steady swimming and turning gaits, and from which propulsive forces can be measured, was determined to be sufficient as a test platform. This will allow for the investigation of the roles of the lateral line and intrinsic fin sensors in pectoral fin control. Eventually, our goal is to construct two pectoral fins attached to a system that can swim freely, hover and change orientation in response to environmental perturbations. This will allow vestibular inputs to be considered in the control of the pectoral fin, and for the role of the fin in the control of the fish body to be explored.

2.1.2. Fin design. The design of the fin was based on robotic pectoral fins developed previously to execute motions appropriate for steady swimming (Tangorra *et al* 2008, 2010) and yaw turns (Gottlieb *et al* 2010). The original systems addressed the gait patterns individually, so a redesign was required for the new fin to produce more complex motions and maneuvering as well as steady propulsion. In all cases, the fin's shape, mechanical properties, and motions were derived from those of biological fins.

The biorobotic fin (figure 1) uses five fin rays to support and move an elastic webbing (80% polyester, 20% elastane) shaped like the biological fin. The linear dimensions of the fin were approximately four times those of a biological pectoral fin. The cross sections of the fin rays were tapered from base to tip such that the flexural rigidities of the fin rays were scaled to those measured from biological fins. This gives the robotic fin bending characteristics across its chord and span similar to the biological fin, and has been demonstrated to have a significant impact on the ability of the robotic fin to create the appropriate propulsive forces, especially thrust during the fin's outstroke (Tangorra *et al* 2010). Sunfish have the ability to actively stiffen their fin rays, but due to the complexity of the mechanisms required to implement active control of stiffness, it is not included in this initial design. Previous implementations were able to control the curvature of the fin ray, but did not regulate stiffness reliably (Tangorra *et al* 2007, Phelan *et al* 2009). Instead, the stiffness of the fin is adjusted by replacing fin rays. Fin rays with flexural rigidities 200 to 1000 times those of the biological fin rays were selected based on results reported in Tangorra *et al* (2010) and Gottlieb *et al* (2010).

To approximate the kinematics used in steady swimming and in turns, each of the five fin rays can be actuated in sweep, and fin rays 1, 2 and 5 (ray 1 being the most dorsal) can also be actuated laterally (figure 1). This allows for expansion, contraction and rotation in the plane of the webbing, for 2D rotational paths to be created. Each fin ray is mounted to a hinge, which allows for sweep forward and back, and the hinges are mounted into an aluminum cylinder that allows for lateral rotations. The fin ray bases are actuated via low-stretch tendons that travel through the center of the aluminum cylinder in order to reduce coupling between the sweep and lateral motions. The tendons are routed to servomotors through mandrel-bent aluminum tubes. This allows the tendons to pass smoothly around the fin's structure, and greatly simplifies tendon tensioning and packaging. The tendons are driven using digital servomotors (HSR-5990TGs, Hitec RCD USA, Poway, CA), which have sufficient torque and speed to flap the fin at frequencies in excess of 2.0 Hz. Tests of the servomotors under load indicated that there was a delay of approximately 0.06 s between the input command and the motor's motion when under load. This delay was assessed to be acceptable for this application and is discussed further in section 4.

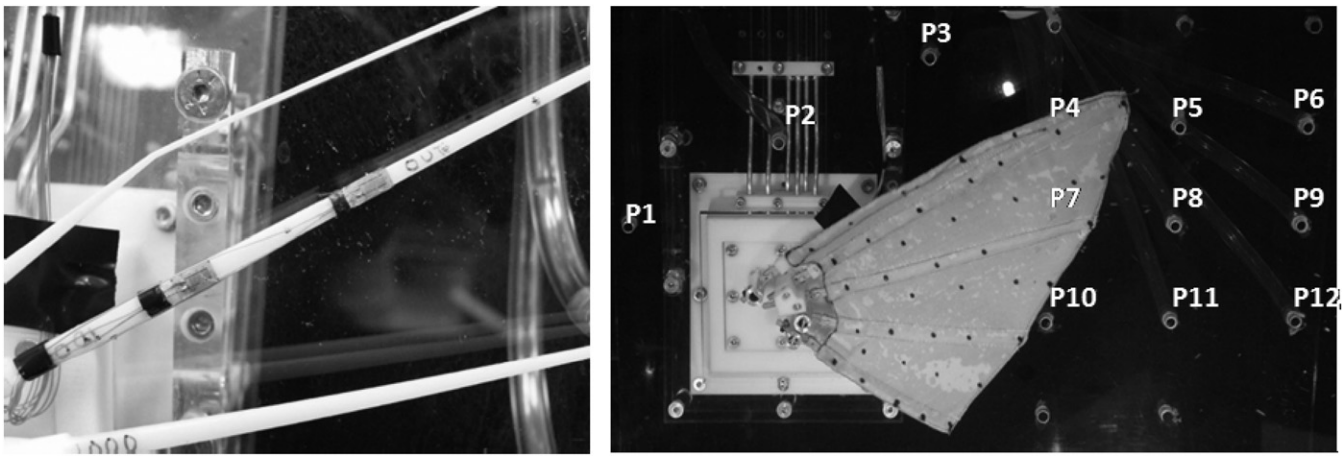

Figure 2. Fin sensors. Strain gages located at 1/3 and 2/3 along fin ray length (left). Ports for pressure measurements along the fin's body plate, which represents the fish body, surface (right).

2.2. *Sensory system*

2.2.1. Functional requirements. The objective is to model the functional performance of the biological sensory systems involved in the closed-loop control of the fin. Fish have numerous sensory systems extrinsic, and potentially intrinsic, to the fin's webbing and musculature. However, the type of information that is sensed by the fin and the extent to which information from sensory systems is used to modulate the fin are almost entirely unknown. Therefore, the requirements for the robotic sensory system are not defined precisely. Instead, an initial sensory configuration was selected to help understand how the hydrodynamic and mechanical information available to the fin was related to propulsive forces.

The sensory systems extrinsic to the fin include the lateral line, the vestibular system and the visual system (Collin and Marshall 2003, Webb *et al* 2008). Of these, the modeling of lateral line function was believed to be the most important. The lateral line senses the fluid pressures across its canal neuromasts and has been shown to encode the frequency content of vortical flows (Liao *et al* 2003, Liao 2006). It is located along the flank of the fish in the region where the vortices created by the pectoral fin develop and are shed. It is, therefore, quite likely that the lateral line provides information about flows shed from the pectoral fin (Mittal *et al* 2006). The vestibular system, which measures the rotational velocities and linear accelerations of the fish body, certainly influences how the fins are used. The modeling of its function will become crucial when the fin is incorporated onto a body that is allowed to move. Inputs from the visual system can also affect fin motions, but the fish is perfectly capable of swimming and maneuvering effectively in the dark or when eye-cups are used to eliminate vision. Thus, vision is likely not crucial for effective, closed-loop modulation of fin ray motions and properties.

The determination of the sensors intrinsic to the pectoral fin is an active area of this research collaboration. Preliminary studies of sunfish have shown that nerves run adjacent to the fin rays and that there are free nerve endings throughout the pectoral fin webbing. It is speculated that these nerves sense the bending of the fin rays and/or flow over the fin. However, since this is speculative, functional requirements for the sensors within the fin were based on the physical phenomena that have been determined to affect fin forces. This includes the driven motion of the fin rays, fin ray stiffness and bending (Tangorra *et al* 2008, 2010), and flow patterns across, or shed by, the fin (Mittal *et al* 2006, Dong *et al* 2010).

2.2.2. Sensory system design. The initial sensory configuration was established to measure flow pressure along the body plate, fin bending, driven fin ray motions and the resultant thrust and lateral forces.

Flow pressure along the body plate is measured using an array of pressure sensors connected to ports distributed across the body plate (figure 2). Port placement was selected to measure pressure in the flow prior to the fin, behind the fin, and downstream where the vortices created by the fin are shed. The pressure sensors (Omega PX26-001DV, Omega Engineering, Stanford, CT) are mounted above the waterline and are connected through plastic tubing to the ports placed along the fin's body plate. The lines running to the pressure sensors are carefully bled to purge all air bubbles before experimentation commences. The power and frequency contents of the signals from the sensors were assessed to ensure that any noise from an oscillation of the water column was low in power and could be distinguished from the signal created by the fin.

Hot film anemometry (HFA) was also evaluated as an alternative to measuring pressure directly. Hot film anemometry has proven to be an excellent tool for identifying critical characteristics of a flow, such as separation, stagnation points and the boundary layer state (Mangalam *et al* 2004). Additionally, the HFA sensor's low profile and flexible configurations are attractive for applications on contoured surfaces, such as a biorobotic fin. Unfortunately, the characteristics of the flow over the fish body that are critical to the closed-loop control of the fin are not yet known. Therefore, it was felt that the expense and complexities associated with using the sensors were too great to justify their use until the relationship between hydrodynamic events and fin forces was

better understood. Furthermore, since the canal neuromasts of the lateral line are considered pressure sensors, the direct measurement of flow pressure was more biologically relevant.

Fin bending was monitored using strain gauges located along the fin ray adjacent to the dorsal leading edge (figure 2) and by using high-definition, high-speed video of the entire fin. Previous studies have shown that the fin's propulsive forces, particularly thrust during the outstroke, are very sensitive to the bending of the long fin rays in the dorsal half of the fin (Mittal *et al* 2006, Dong *et al* 2010). Of the two long, flexible fin rays within the dorsal half of the robotic fin, fin ray 2 was selected since its deformations were affected by deformations of the leading edge and of the fin tip, both of which are important to the production of thrust forces.

Two strain gauges (Omega SGT-3S/350-TY13) are arranged in a half bridge configuration, and fixed to both sides of the fin. Two sets of two gauge elements were positioned 30 and 60 mm from the fin ray base. These locations were selected so that changes in curvatures along the length of the fin would be monitored and so that the strain of the gauge would be within the limits of the sensor. The strains and resulting curvatures were validated against the high speed video of the fin's motions. The strain bridge outputs are processed using a strain gauge module (SCC-SG03, National Instruments, Austin, TX) which includes excitation and offset nulling circuitry along with a 1.6 kHz low-pass filter.

Thrust and lateral forces generated by the flapping fin are measured using S-beam load cells (Futek LSB200, Futek Advanced Sensor Technology, Inc., Irvine, CA) that connect the biorobotic fin assembly, which is supported by air bearings (New Way S301301, New Way Air Bearings, Aston, PA), to ground. In addition to being used to establish a relationship between the sensory information, fin motions and the propulsion forces, the force data were used to validate that the biorobotic fin had produced biologically relevant forces and motions.

2.3. Controller

2.3.1. Functional requirements. The controller is the main computational element for investigating and ultimately enabling, effective closed-loop control of the pectoral fin. Its functions include data acquisition, signal processing, sensor fusion, decision and control computations and generating command inputs for the fin ray actuators. Since the sensory systems with which the controller interacts cannot be specified fully, and the control strategy and its computational demands are unknown, a core requirement was for the system to be reconfigurable and scalable so that it could adapt as the sensory and computational demands changed.

The system must be capable of acquiring data from many sensors of varying types. The exact number and types are not well defined, but are expected to include both digital and analog signals from strain gages (fin bending), pressure sensors (flow information), motor encoders and power monitoring, forces gages, accelerometers and velocities (orientation) and other sensors that will be identified in the neurobiological studies. Signal processing will include, at a minimum, signal conditioning and sensor fusion. Some of this processing is expected to occur in parallel, external to the control sequence, so that relevant information made from the data can serve as an input to the control strategy. The controller must be powerful enough, and have sufficient memory, to accommodate and execute both traditional and biologically derived control strategies. This may include open-loop command of fin motions, closed-loop control of fin gaits and speeds based upon body orientation, central pattern generators (Ijspeert 2008, Seo *et al* 2010) that drive individual fin rays and are modulated via sensory information and also the exploration of new control architectures that may be derived directly from the neurobiological investigations of the pectoral fin. The signal processing and computational requirements should be facilitated using a programming language that is user friendly, that has rigorous high-level functionality, and that accepts custom scripts for mathematical coding (e.g., Matlab or Labview). Lastly, the system must be able to create motor control outputs (e.g., PWM or analog) for a minimum of eight actuators in a very basic fin, to 15 to 20 in a fin with 3 DOF, and up to 40 when two pectoral fins are implemented on a moving body. Based on robotic fins that operate at up to 2 Hz, and having minimum of 20 position updates per cycle, the control system must acquire data, process the signals, execute the controller computation and update command signals at an estimated minimum of 40 Hz.

2.3.2. Controller design. Data acquisition, processing and motor control are conducted using a National Instruments PXI-8106 real-time controller with two M-series 6229 DAQ cards and one M-series 6723 DAQ card (National Instruments, Austin, TX). This provides 96 digital I/O channels, 40 analog out, 64 analog in, 12 dedicated strain gauge channels, four 80 MHz hardware clocks and a 2.16 GHz dual core processor. Four slots are available for system expansion and the implementation of I/O cards with dedicated field-programmable gate arrays. This allows for in-line, parallel processing and fusion of sensory information external to the control loop. Programming is conducted using Labview Real Time and FPGA programming. It has the adaptability of the standard Labview libraries with deterministic control loops, parallel processing by FPGAs, and the inclusion of scripts programmed in Matlab (The Mathworks Inc., Natick, MA) and C/C++.

The system is currently configured to generate the signals to drive the fin ray servomotors directly and to acquire data from pressure sensors, strain gauges, load cells and commanded positions. The servos require pulse width-modulated (PWM) signals to operate, these signals are updated at a 90 Hz rate, which is the fastest the servos can tolerate. Sensory data are acquired at 200 Hz, stored in RAM during experimentation and written to file once the experiment concludes. The program is configured such that it can be easily modified to have sensory data modify the fin ray trajectories and to include more motors and sensors. During experimentation, this configuration rarely used more than 10% of the available processing power.

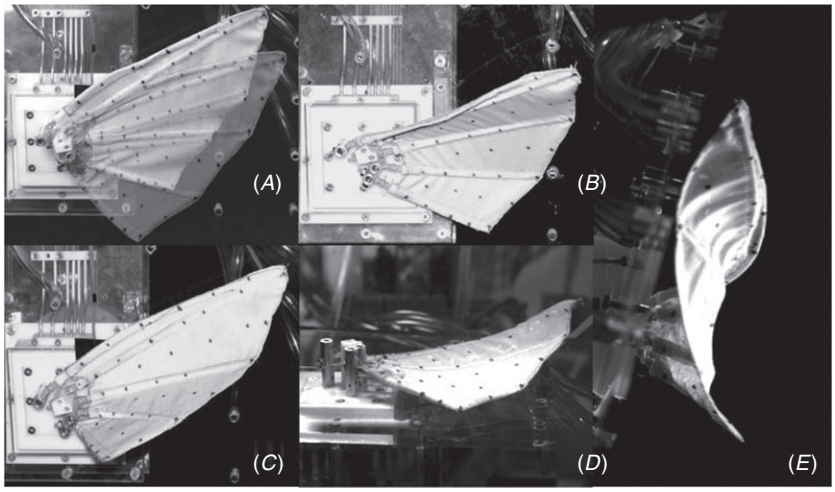

Figure 3. Fin motions. The two actuated degrees of freedom in each fin ray allows for rotation, expansion and contraction of the entire fin, shown as a double image of two fin positions (*A*). The independent control of the fin rays in the upper (*B*) and lower (*C*) lobes provides sufficient control to generate maneuvering and steady swimming motions. The fin generates the appropriate cupping shape characteristic of the steady swimming gait (*E*) but the webbing does not fully reattach to the body plate at the end of one beat before beginning the next (*D*).

3. Experimentation and methods

Experiments were conducted to evaluate the performance of the fin and to investigate relationships between steady swimming propulsive forces, the movements of the fin rays and the sensory information available for closed-loop control of the fin. The motions, forces and sensory information (commanded fin ray positions, fin ray curvatures, and flow pressures) produced by robotic fins with four flexural rigidity configurations (200×, 400×, 800×, 1000×) were evaluated. Fins were operated at flapping frequencies of 0.50, 0.65, 1.00, 1.30 and 1.60 Hz in a flow of 90 mm s^{-1}. This corresponded to Strouhal numbers that ranged from approximately 0.7 to 2.3. The four fins were also operated at flapping frequencies of 1.00 Hz in flows of 56, 69, 140 and 180 mm s^{-1}, which correspond to the same range of Strouhal numbers.

As described in Tangorra *et al* (2007), the biorobotic fins were supported from a carriage that was mounted to the top of a rectangular flow tank. The carriage rested on eight precision air bearings (New Way S301301, New Way Air Bearings, Aston, PA), and could translate fore, aft and laterally, or be fixed against two s-beam load cells (LSB200, FUTEK Advanced Sensor technology, Inc., Irvine, CA). This arrangement allowed thrust and lateral forces to be measured simultaneously. The magnitude and direction of the 2D force were calculated by combining the thrust and lateral forces vectorially.

Data were collected at 200 Hz using a National Instruments PXI M-series 6229 data acquisition board (National Instruments Corp., Austin, TX) and low pass filtered at 10 Hz. The low pass filter was designed using the Kaiser window method to have a pass-band frequency of 10 Hz, a stop-band frequency of 12 Hz and a peak error of 10^{-4} (Oppenheim *et al* 1999). Representative results for the forces, strains and pressures produced during the stroke cycle (outstroke, instroke) were calculated by averaging forces from six stroke cycles. Standard errors were calculated for each mean force curve.

The results presented are representative of those created during the repeated, cyclic flapping. Data from the first fin beats were omitted so that transients were not included in the analysis. However, for clarity, the results are presented as if the data began from rest. This was done so that the timing between different signals and data sets could be seen clearly (figure 4).

High resolution (1024 × 1024 pixel), high speed (250 fps) video were used to document fin kinematics. The procedure that was followed was documented in Standen and Lauder (2005). Three synchronized cameras (Fastcam, Photron USA, Inc.) calibrated in three dimensions using direct linear transformation and a series of mirrors were arranged to capture the dorsal, lateral and posterior views of the fins.

4. Results

4.1. Fin motions

The robotic fin executed good approximations of the biological steady swimming and yaw turn maneuver gaits, and had sufficient actuated degrees of freedom to adjust movements of individual fin rays so that the fin's kinematics could be adjusted to manipulate propulsive forces. The movements of the fin were evaluated as the fin was flapped in air and water for both gaits. In steady swimming, the biorobotic fin executed the dominant cupping and sweep motions (Tangorra *et al* 2007) of the biological fin's gait at the fin's base (figure 3), and the flexibility of the fin rays and fin webbing allowed the fin to bend back during the fin's outstroke and to have an appropriate dynamic interaction with the water. In maneuvering, the biorobotic fin exhibited independent control over the upper and lower lobes of the fin and the ability to rotate, expand and contract the entire fin (figure 3). Although the motions of the biorobotic fin were visually similar to the biological fin, the driven motions of the fin rays were not intended to model the full kinematics used by the biological fin. As described

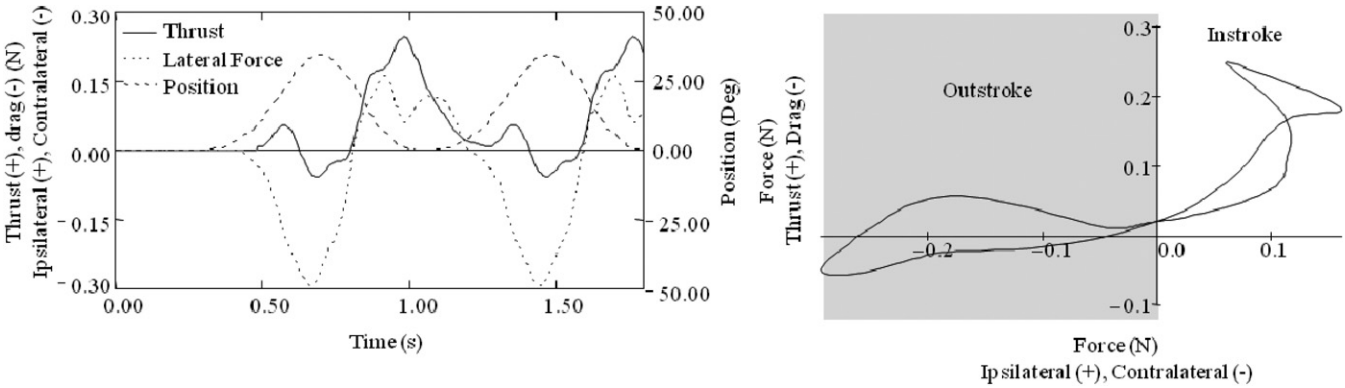

Figure 4. Thrust and lateral forces produced by the robotic fin (standard deviations less than 1% of average and error bars are therefore removed for clarity). Representative thrust and lateral forces are shown versus time relative to the commanded position of the fin rays (left). Note that there is a single large thrust peak, and a small drag phase during the fin beat cycle. Thrust versus lift plot (right) shows how fish would be affected by the fin forces. The data are from a fin with fin rays scaled 800×, flapped at 1.3 Hz, and in a 90 mm s^{-1} flow.

in detail in Tangorra *et al* (2007), the biological motions were decomposed into orthogonal modes and the trajectories of the most dominant modes were used for the motions of the robotic fin. When combined with flexible fin rays, these simplified movements generated the majority of the forces predicted for the biological fin.

The accurate control of the fin's motions was largely due to the effectiveness of the 2D rotary axes on which the fin rays were mounted (figure 1, part C). The design of the rotary axes—which allowed the tendons that drove sweep motions to pass through the axis centerline—enabled rotations in which no coupling was evident between the sweep and lateral (perpendicular to sweep) motions. This permitted easy control and adjustment of the 2D trajectories required to execute the turn maneuvers (figure 3). The mechanism also had a large range of motion, which made it possible for the upper half of the fin to contract and expand (movement toward and away from the midline) by 15° and the lower half by 25°. This allowed the entire fin to be reoriented so that the direction of the propulsive forces could be more carefully modulated. Furthermore, the compact design of the rotary mechanism and tendon passages allowed the fin ray base geometry to be curved similarly to that of biological pectoral fin girdle. This appropriate geometry was important for the fin rays to move through the appropriate paths.

During the experimental trials in which the fin was cycled, the biorobotic fin's webbing did not fully return to the body at the end of the instroke (figure 3, panel D). Although the base of the fin did indeed complete the instroke and return to the body plate, the fin began the subsequent outstroke before the motion of the fin tip had stopped and reattached to the body plate. This was caused by setting the duration of the pause between fin beat cycles too short in experimental test trials and was discovered during the analysis of the video data. The failure of the fin webbing to reattach to the body plate affected the thrust produced by the fin during the outstroke; this is clear when comparing the outstroke thrust during the first cycle of a trial, in which the webbing is attached to the body plate before fin movement commences, to the following cycles. The outstroke thrust force is consistently higher during the first fin beat of a trial and the difference between the outstroke thrust during the first cycle and consecutive cycles becomes more pronounced as the flapping frequency increases. It was demonstrated in Tangorra *et al* (2010) that outstroke thrust is very sensitive to fin ray movements and bending, therefore this finding is expected. Although this portion of the fin's motion during the experimental trials was not ideal, the motion did not corrupt the sensory measures. The force profile may have been affected, but the relations between sensory information and forces are still valid.

4.2. Propulsive forces

The forces produced by the biorobotic fin were consistent with those predicted using CFD models (Mittal *et al* 2006), evaluated through studies of the sunfish (Lauder *et al* 2006) and determined experimentally using other biorobotic fin models (Tangorra *et al* 2008). These data are the first biorobotic measures of the pectoral fin's lateral forces during steady swimming. Previously, only thrust and lift forces were measured. During steady swimming, the fin's outstroke produced a contra-lateral force and a smaller peak of thrust (figure 4). Occasionally, the thrust force transitioned to drag partly through the outstroke. During the instroke, the fins produced an ipsi-lateral force and a thrust force of similar magnitude. The tendency would be for the forces from a single pectoral fin to push the fish, or an AUV, slightly forward and contra-laterally during the outstroke, and then forward and ipsi-laterally during the instroke. In reality, the fish is propelled forward during the fin's outstroke and instroke, but the lateral forces are balanced by lateral forces from the other pectoral fin. The maneuvering stroke altered the forces so that a much stronger lateral force and a negative thrust were created during the outstroke. Instroke forces were similar to steady swimming, but lower in magnitude.

Propulsive forces were sensitive to fin ray stiffness and to the fin's operating conditions (figure 5). In general, when flapping frequency or fin stiffness was increased, the average magnitude of the 2D force (vectorial combination of the thrust and lateral force) and the lateral force increased during both the outstroke and instroke, and the average magnitude of the thrust

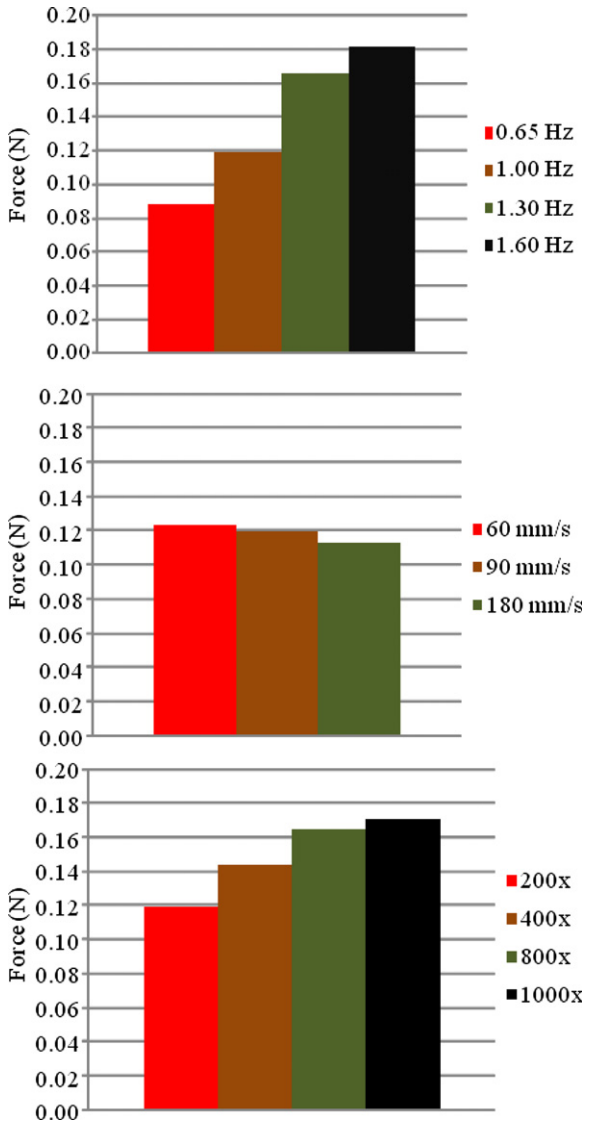

Figure 5. Representative average magnitudes of the 2D propulsive force over a full fin beat as flapping frequency of the 800× stiffness fin was changed (top), as the flow rate of 800× fin at 1.3 Hz was changed (middle), and as stiffness (bottom) of the fin at 1.3 Hz was changed (bottom). Trends for thrust and lateral forces were similar over full fin beat.

increased during the instroke. As the flow rate was increased, the average magnitude of the 2D and the lateral force increased during the outstroke, and the average magnitude of the 2D, lateral, and thrust decreased during the instroke. This resulted in the 2D force decreasing over the full fin beat as the flow rate was increased. Trends for thrust during the outstroke were not as clear. Thrust during the outstroke was very sensitive to the bending of the fin. Despite the fact that a stiffer, albeit still very flexible, fin will produce a greater overall 2D force, the more flexible fin may often produce a higher peak thrust. This was due to how the overall force produced by the fin was directed into the water. Overall, the relations were consistent with those described in detail in Tangorra *et al* (2010). A lag existed between the commanded motions of the fin ray actuators and the forces produced by these very flexible fins (figure 6). This lag typically measured between 100 and 300 ms, which for the faster flapping frequencies could be over a quarter of the fin beat period. For a fin of a given stiffness, the lag increased approximately parabolically with the period of the flapping cycle and included a constant delay (figure 6). At certain frequencies and flows, the total lag increased as fin stiffness decreased, but only by a small amount. For example, the lags for the most compliant fin (200×) were only several hundredths of a second longer than for the stiffest fin (1000×). This trend persisted in less than half of the trials though and, because of the small amounts of the change, may indicate that fin stiffness may not be the only contributor to the variable portion of the lag. The total lag can be decomposed into three components: a delay between the commanded motion and the movement of the servomotor, a delay between the movement of servomotor and the movement of the fin ray and delay that was proportional to the period of the flapping cycle. The gain of this third portion was a function of fin ray stiffness. The delay between the motor command and the motion of the servomotor was measured experimentally to be approximately 50 ms. This was measured while the motor was under a moderate load, and is expected to vary slightly as the load changes. The delay between the motor command and the motion of the fin ray was measured experimentally to be approximately 50 ms, and is attributed to the movement, and tensioning and un-tensioning of the tendons during a motion. The delay caused by the

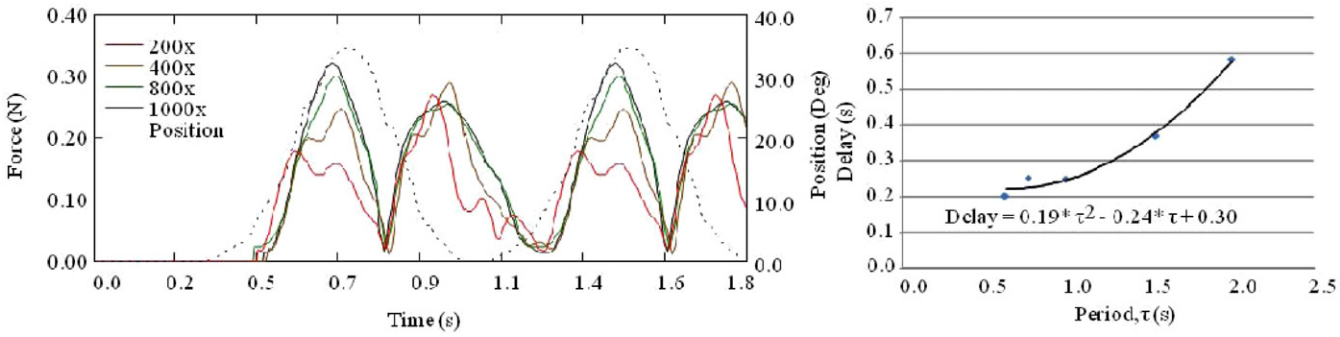

Figure 6. Propulsive forces lag fin ray motions. Magnitude of 2D force for fins flapped at 1.30 Hz in 90 mm s^{-1} of flow (left). At this frequency, the propulsive force of the fin lagged the commanded position by nearly 0.25 s. The lag increased by only a small amount as the fins became more compliant. The lags increased approximately parabolically as the cycle period increased (right).

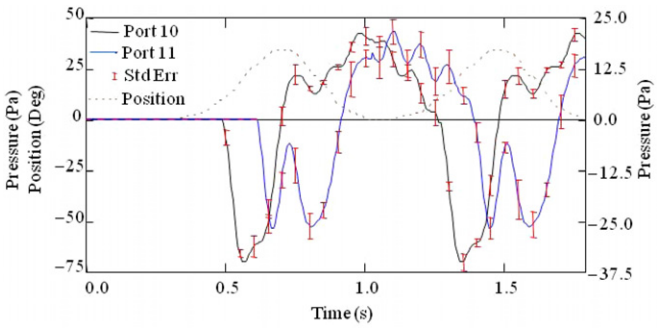

Figure 7. Fluid pressure downstream of a 1000× stiffness fin. The fin was flapped at 1.3 Hz in a flow of 90 mm s^{-1}. There are considerable differences in the magnitude and delay of the signals measured at ports 10 (solid) and 11 (dashed), but the structure of the pressure signal is similar between the two ports. Port 11 is located 60 mm downstream of port 10. The sampled commanded position (dotted) is included for reference.

tendons is not constant throughout the fin beat and is expected to be a maximum when a tendon that is not under tension is loaded due to the reversal of the direction of rotation of the servo. Furthermore, this delay may vary in proportion to fin loading because of tendon stretch. This may help explain why lags did not trend reliably with stiffness. Although the lag due to the fin's compliance is expected to decrease with the stiffness of the fin, the additional force produced by the stiffer fin increases loading on the tendons which may cause the tendons to stretch and therefore increase lag.

4.3. Fluid pressure along fish body

Significant changes in fluid pressure due to the motion of the fin were measured at ports downstream of the fin (figure 2), while little change in pressure that could be attributed to the motion of the fin was sensed upstream of the fin. The most significant pressure changes were detected consistently along the line sensed by sensors 10, 11 and 12. The ports for these sensors were located slightly lower than the fin's midline when the fin was against the body plate, and were in line with the fin's dorsal edge when the fin was swept forward and cupped at the end of the outstroke. These ports were likely near the region where the vortices shed by the fin at the end of the instroke and outstroke were located (Mittal *et al* 2006, Dong *et al* 2010). An analysis of the spectral content of the pressure signals indicated that the frequency at which these signals had the most power coincided with the fin's flapping frequency and its harmonics. These results are evidence that the measured signals were the result of the fin's flapping, rather than an artifact from oscillations of the water columns within the tubes that connect the open port to the pressure transducers.

In general, the magnitude of the pressure signal cycled with the outstroke and instroke of the fin. As the fin was flapped, the measured pressure dropped from the free stream value, reached a negative peak, then increased, reached a positive peak that was broader than the negative peak, and decreased back to the free stream value (figure 7). At port 10, which was immediately downstream of the fin, the timing of the peak pressures correlated well with the timing of the 2D propulsive force (vectorial combination of the thrust and lateral forces), and in particular, the peak negative pressure occurred closely to the peak in the outstroke thrust (figure 8). The same structure was evident in the pressure signals measured at the majority of the sensors downstream of the fin. As the flow moved downstream, the magnitude of the pressure peaks tended to decrease, the shape of the peaks became less defined and the delay between the propulsive force and the occurrence of the pressure signal became longer (figure 7). In some instances, the negative pressure pulses exhibited a 'double peak'. These double peaks might be explained by an oscillation internal to the flow structure or to destructive addition of flow events emanating from other portions of the fin, but it is not currently known why this shape exists. Experiments in the future will attempt to clarify the structure of the pressure in the wake flow from the fin. CFD studies performed on the flapping of the pectoral fin of the bluegill sunfish (Dong *et al* 2010) indicate that the flow structure downstream of the fin is quite complicated.

In the majority of trials, the magnitudes of the two pressure peaks increased with increases in the fin's flapping frequency, the flow rate and fin ray stiffness (figure 9). The pressure increases were more consistent for the negative pressure peak, which was the result of the fin's outstroke, than they were for the positive peak, which was caused by the fin's instroke. During the fin's outstroke, the increases in pressure coincided with changes in the 2D force, which increased with flapping frequency, fin stiffness and flow rate (figures 9 and 10). For example, when the fin with an 800× stiffness was flapped at 1.0 Hz in 90 mm s^{-1} of flow, it produced an average 2D force during the outstroke of 131 mN and had a peak pressure magnitude of 70 Pa (figure 10). When its fin beat was increased to 1.60 Hz, the average outstroke force increased to 176 mN and the magnitude of the peak pressure increased to 96 Pa. When the stiffness of the fin was increased to 1000× (1.0 Hz), the average outstroke force increased to 139 mN and the peak pressure increased to 80 Pa. When the flow rate was increased from to 180 mm s^{-1} for the 800× fin flapped at 1.0 Hz, the peak pressure magnitude increased to 96 Pa, and the average outstroke force increased to 144 mN. Instroke 2D forces followed a similar trend, increasing with increases in flapping frequency and stiffness, but decreased with increasing flow.

The pressure signal propagated along the body plate significantly faster than the velocity of the flow. For example, propagation speeds ranged from 260 to 1500 mm s^{-1} for the 800× fin in 90 mm s^{-1} of free stream flow. It was hypothesized that the propagation speed would increase as the force generated by the fin increased due to the fin accelerating the flow. However, this was not consistently the case when fin forces increased through increases in fin stiffness and flapping frequency, or through decreases in flow speed. For example, as the flapping frequency of an 800× fin was increased from 0.50 to 1.00 Hz, the propagation speed increased from 260 to 1500 mm s^{-1}, but when the flapping frequency was then increased to 1.60 Hz, the propagation speed decreased from

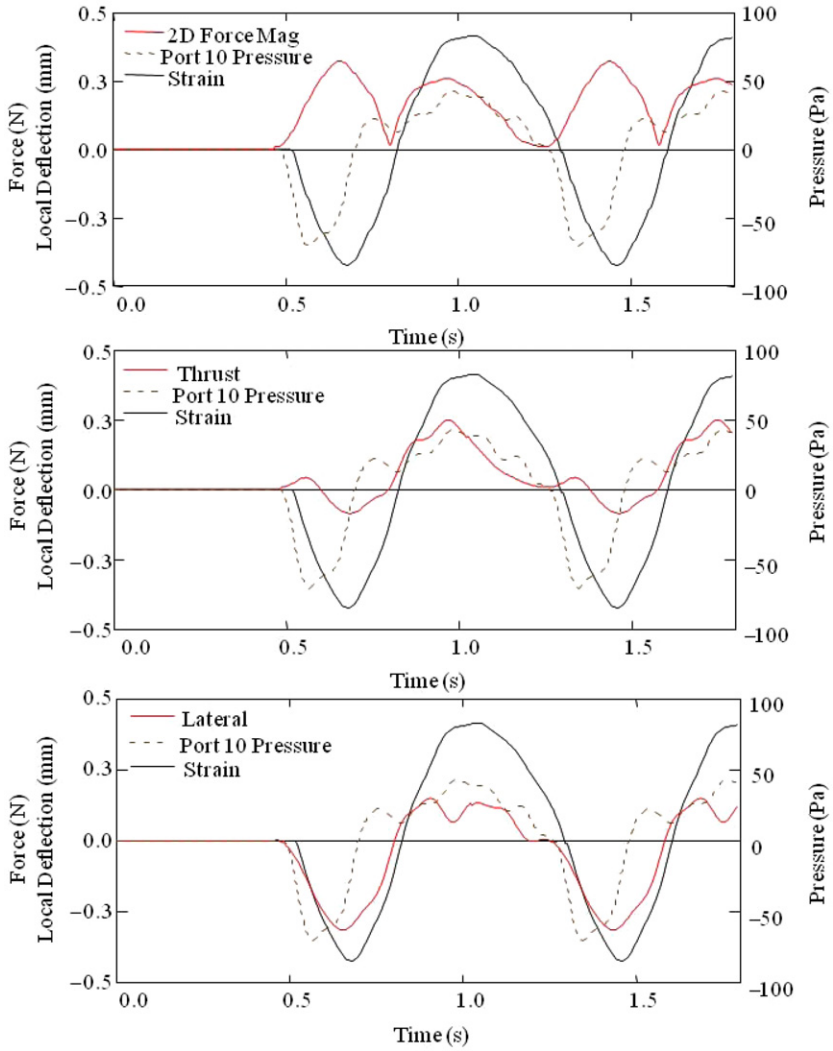

Figure 8. The alignment of the force (red), pressure at port 10 (brown), and strain profile for a 1000× fin flapped at 1.3 Hz. The magnitudes are shown for the 2D force (top), thrust (middle) and lateral forces (bottom).

1500 to 290 mm s^{-1}. Additionally, propagation speed was often higher for fins of lower stiffness than for fins of higher stiffness when the fins operated at the same flapping frequency and flow rate. To ensure that these observations were not created by the analysis technique, several methods were used to determine the time difference between pressure signals: the lag of the peak of the cross-correlation function between the two pressure signals (Bendat and Piersol 2000); the mean square error between the averaged pressure signals; the mean square error using three cycles of unaveraged pressure data; the mean square error between regions of the pressure signal around the peaks and visual alignment of the signals. The same patterns were found using all these techniques. Ultimately, propagation speed is an interesting phenomenon that supports the hypothesis that the pressure signals are caused by the fin's action, not by the freestream flow. Relating propagation speed to fin forces and to experimental conditions will require further research and experimentation.

4.4. Fin ray bending

The bending of the fin rays was dependent on the magnitude of the force produced by the fin, the direction of the force and the stiffness of the fin rays. The bending of these very flexible fin rays tracked the magnitude of the fin's forces closely (figure 8). Overall, as the propulsive forces developed during the outstroke, the bending of the fin ray increased, peaked just after the peaks of the outstroke forces, then reversed direction and peaked just after the peaks of the instroke forces. The bending of the fin rays, at both the bottom and mid-point of the ray, lagged the 2D forces by a small amount, usually by less than 50 ms.

For fins of a given stiffness (e.g., 800×), the curvature of the fin rays increased during both the outstroke and instroke as the fin's flapping frequency was increased and as the flow rate was decreased (figure 11). The changes were not large, but the trend occurred in all fins. This is consistent with increases in the fin's 2D propulsive force. However, the decrease in

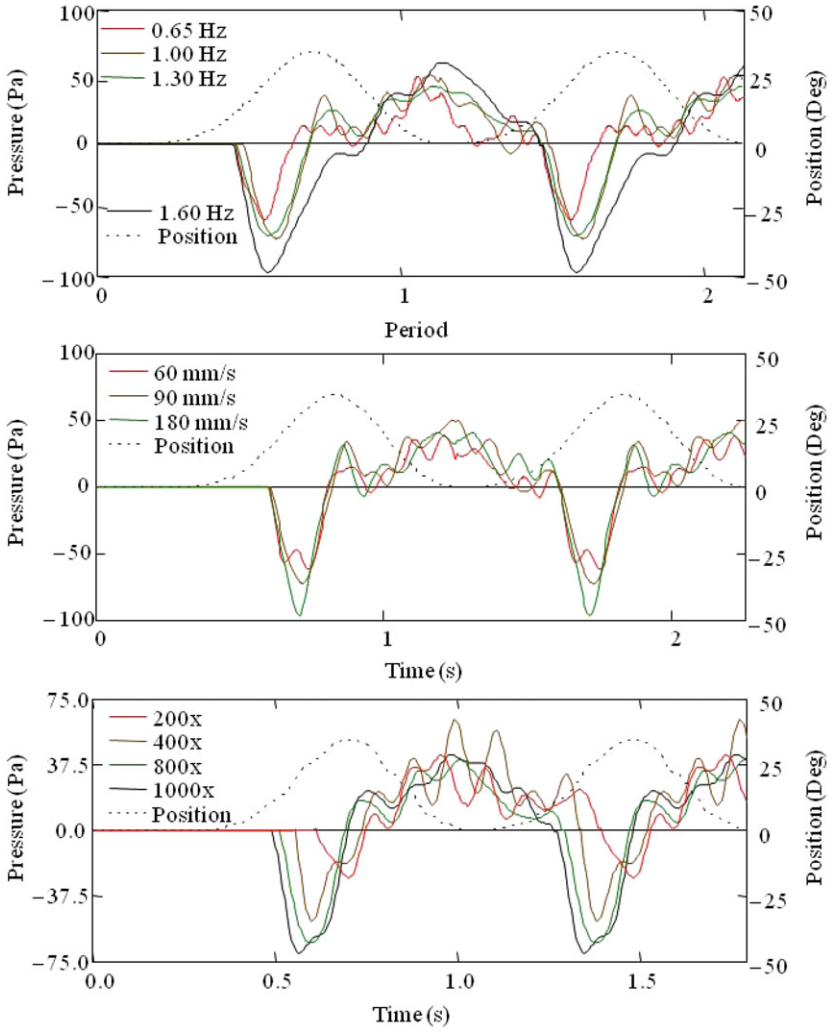

Figure 9. Representative fluid pressures as the flapping frequency of 800× fin was changed (top), as the flow rate of 800× fin at 1.3 Hz was changed (middle) and as stiffness (bottom) of fin at 1.3 Hz was changed (bottom). Curves for 0.50 Hz, 70 mm s^{-1} and 140 mm s^{-1} data sets were removed for clarity.

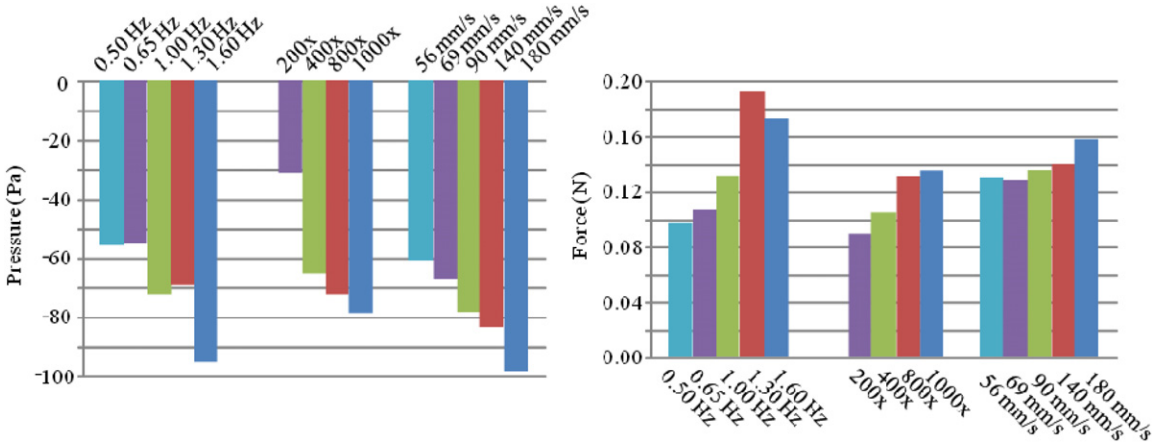

Figure 10. Peak pressures measured at port 10 (left), average 2D force during the outstroke (right). Peak pressure and 2D outstroke force both increase with increasing frequency (800× fin in 90 mm s^{-1} of flow), stiffness (flapped at 1.30 Hz in 90 mm s^{-1} of flow) and flow (800× fin flapped at 1.0 Hz).

bending during the outstroke as flow speed was increased is somewhat counterintuitive. It was expected that an increase in the velocity of the water past the fin would cause the fin to bend back more, but this was not the case.

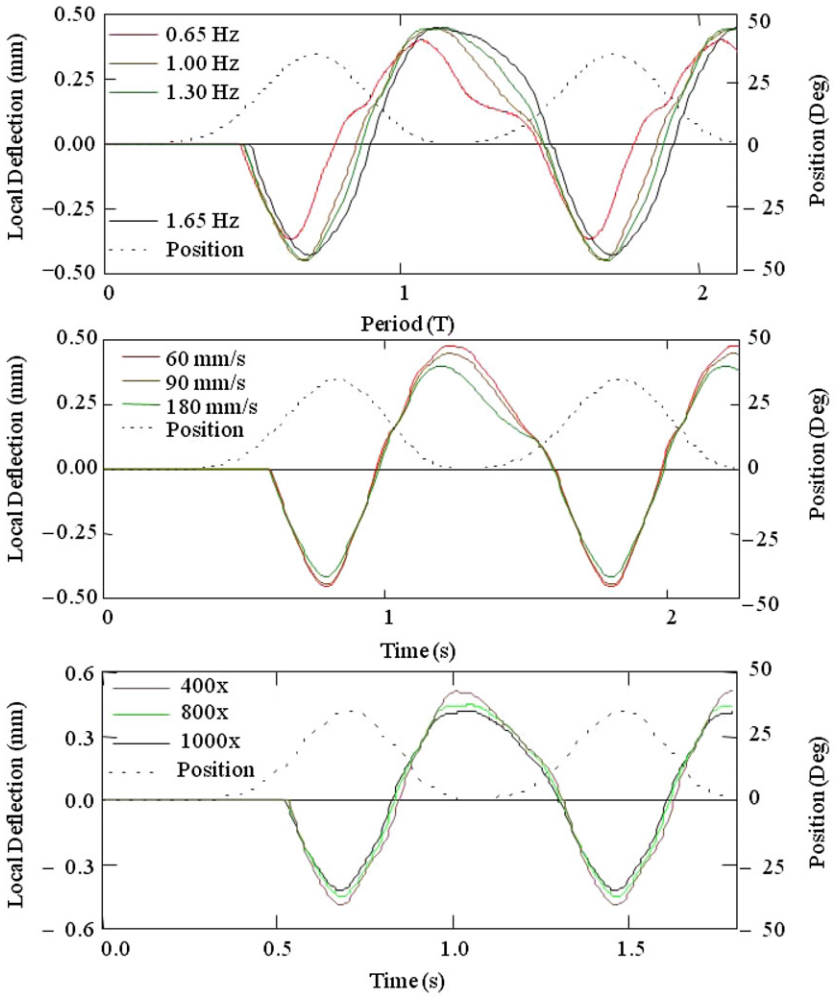

Figure 11. Differential strains measured near midpoint of fin ray 2. Differential strain is a measure of bending. Strains for the 800× fin flapped at different frequencies in 90 mm s^{-1} of flow (top). Strains for the 800× fin flapped at 1.0 Hz in different flows (center). Strains for fins of different stiffness flapped at 1.3 Hz in 90 mm s^{-1} of flow (bottom).

For fins of different stiffness that were operated at the same flapping frequency and flow rate, fin ray bending decreased as fin ray stiffness increased (figure 11, bottom). For example, the magnitude of the average and peak strains of a 400× fin were greater than the average and peak strains in the 1000× fin, but the 1000× fin produced significantly greater force. In these cases, the forces produced by the stiffer fin did not increase as rapidly as the fin's resistance to bending, and therefore the bending did not increase as forces rose. The reduced bending of the stiffer fin altered the direction of the fin's propulsive force as well, and may explain why peak thrust during the outstroke was often larger for more compliant fins. Although the average 2D forces increased with increases in fin stiffness, the stiffer fins did not bend back as much during the outstroke, and thus did not push the flow backward to create thrust during the outstroke. Thus, a greater portion of the 2D force was directed laterally (figure 12).

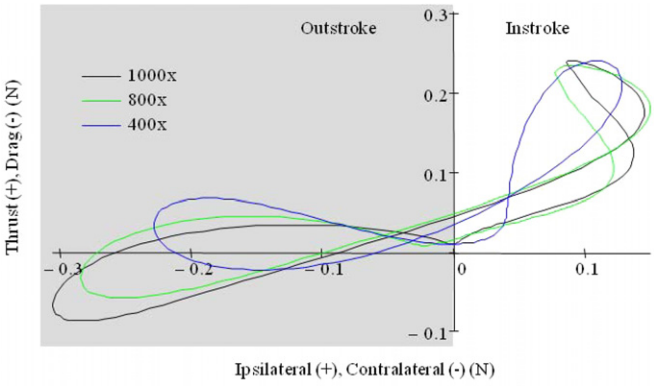

Figure 12. Thrust versus lateral force at 1.3 Hz. For clarity, data were low pass filtered at 5 Hz. Note the increasing thrust force in the outstroke (third quadrant) as stiffness decreases.

If coupled to additional information, the bending of the fin rays could provide a great deal of information about the current propulsive forces. Although fin ray bending does not scale directly with fin force, if the fin ray stiffness were known, changes in the magnitude of the force could be understood from changes in the fin's bending. Furthermore, the curvature of the single fin ray provided some information about the

direction of the force. It is believed that, by instrumenting more fin rays and developing a model from which the curvature of the entire fin could be determined, the direction in which the propulsive force acts on the fluid could be found throughout the fin's beat.

5. Concluding remarks

A biorobotic model of the sunfish pectoral fin and fin sensorimotor system was developed and demonstrated to be a very capable tool for investigating relationships between biologically based sensory information and the fin's propulsive forces. These relationships are necessary for establishing the relevance of potential sensory information to the motions and forces of the pectoral fins, and for providing insight into how the fish may use sensory information in pectoral fin control. This first-generation fin is able to produce motions and forces like the sunfish fin during steady swimming and maneuvering gaits, and can modulate propulsive forces through independent control of the kinematics of its five fin rays. The robotic fin's initial sensory configuration is based on the fish's lateral line and on preliminary data that suggest that the pectoral fin has an intrinsic sensory response to bending. A real-time controller is used for data acquisition and control computation, and can be configured with dedicated field programmable gate arrays (FPGAs) for inline, parallel processing of sensory information external to the control loops that drive fin ray motion. This structure allows for sensor fusion and control strategies to be developed that are derived from the architecture of the fish sensorimotor system.

The forces produced by this biorobotic fin model were consistent with those predicted using numerical models and experimental studies of the fish and of previous biorobotic fins. These data are the first biorobotic measurements of the pectoral fin's lateral forces during steady swimming. Previously, only thrust and lift forces had been measured. Like lift forces, the lateral forces increased with flapping frequency and fin stiffness, and had magnitudes that were on the same order as the thrust forces. The propulsive forces lagged the motor commands and the movements of the fin. Part of the delay was due to a delay in the response of the motor to its command input, and another part was due to the tensioning and relaxation of the tendons as they pulled upon the loaded fin rays. These components of the delay can be reduced through design changes, but cannot be removed altogether, and are counterparts to the delays found in biological systems due to sensor processing and signal transmission along nerves. The more interesting part of the delay was due to the flexible fin. Results from this initial study support that this component of the delay decreased as the frequency at which the fin was flapped increased, but did not reliably increase with increasing compliance as expected. It is believed that the delay does increase with increasing compliance, but because generated force also decreases with increasing compliance, tendon stretch decreases as well and therefore affects the delay in an opposing manner. These delays, and how they change with operating conditions, must be understood and modeled so that the feedback controller can be designed to reduce the impact of the delay on the output error.

The pressure in the flow along the fin's body plate, and the bending of the fin ray in the fin's dorsal half, were related closely to the time-varying force that was produced by the fin (figure 8). The magnitude of the peaks in the pressure signals generally increased as the fin's force increased and the frequency content of the pressure signal also matched that of the fin ray motion and force. The amount of bending of the fin ray also increased as the force generated by a fin of a specific stiffness increased. However, the bending of a very stiff fin was often less than the bending of a more compliant fin that produced less force. Therefore, fin ray bending, without knowledge of the fin ray's stiffness, cannot be used as an absolute measure of force. The amount of bending, independent of stiffness, did, however, correlate with the direction the 2D force and therefore with the relative strengths of the thrust and lateral components. The results strongly suggest that sensory measures of pressure along the body and of fin ray bending are relevant to predicting the fin's force vector and should be pursued for closed-loop control through additional biological and biorobotic studies. In subsequent biorobotic designs, the fidelity, density, and distribution of the pressure and bending sensors will be increased to give us the ability to create a somatosensory map of pressure across the body and of the fin's 3D curvature. Studies that measure the sensory and behavioral response of the biological fin to mechanical and hydrodynamic perturbations will be used to validate the relevance of the biorobotic findings to the biological system.

It is clear from the results that relationships between the fin's propulsive forces and the sensory information are complex. Even for the relatively small number of sensors used in this first generation robotic system, a great deal of information is available in the measured pressure and bending signals. These data must be integrated to form a picture of the force created by the fin and to determine how the fin rays should be modulated to adjust force. The bending of the fin gives an indication of the direction and magnitude of the force, and the pressure sensors give an indication of the magnitude and frequency content of the propulsive force along with the velocity of the flow generated by the fin. However, this information is insufficient without an understanding of the fin's compliance, and both pressure and fin bending would benefit from a much greater number and broader distribution of sensors. This sensory picture will likely become more complex as more of the biological fin's sensory system is uncovered and additional sensory modalities are included in the biorobotic model. Machine learning techniques (Alpaydin 2004) may provide the right framework for developing models that make sense of the coupling between sensory modalities and that connect the relevant sensory information to the fin forces and fin ray motions. It then becomes a question to determine how to relate the algorithm-based machine-learning models to the actual biological framework, and how to use the resultant sensory information within a biologically derived control strategy such as a central pattern generator (Ijspeert 2008).

References

Alben S, Madden P G and Lauder G V 2007 The mechanics of active fin-shape control in ray-finned fishes *J. R. Soc. Interface* **4** 243–56

Alpaydin E 2004 *Introduction to Machine Learning* (Cambridge, MA: MIT Press)

Bendat J and Piersol A 2000 Random data analysis and measurement procedures *Meas. Sci. Technol.* **11** 291–3

Colgate J and Lynch K 2004 Mechanics and control of swimming: a review *IEEE J. Ocean. Eng.* **29** 660–73

Collin S and Marshall N 2003 *Sensory Processing in Aquatic Environments* (New York: Springer)

Coombs S and Van Netten S 2006 The lateral line system *Fish Biomechanics* vol 23 ed R Shadwick and G Lauder (New York: Elsevier) pp 103–39

Dong H, Bozkurttas M, Mittal R, Madden P and Lauder G 2010 Computational modelling and analysis of the hydrodynamics of a highly deformable fish pectoral fin *J. Fluid Mech.* **645** 345–73

Gottlieb J, Tangorra J, Esposito C and Lauder G 2010 A biologically derived pectoral fin for yaw turn manoeuvres *Appl. Bionics Biomech.* **7** 41–55

Ijspeert A J 2008 Central pattern generators for locomotion control in animals and robots: a review *Neural Netw.* **21** 642–53

Lauder G, Madden P, Mittal R, Dong H and Bozkurttas M 2006 Locomotion with flexible propulsors: I. Experimental analysis of pectoral fin swimming in sunfish *Bioinsp. Biomim.* **1** S25–34

Liao J 2006 The role of the lateral line and vision on body kinematics and hydrodynamic preference of rainbow trout in turbulent flow *J. Exp. Biol.* **209** 4077

Liao J, Beal D, Lauder G and Triantafyllou M 2003 The Karman gait: novel body kinematics of rainbow trout swimming in a vortex street *J. Exp. Biol.* **206** 1059–73

Maeda N, Miyoshi S and Toh H 1983 First observation of a muscle spindle in fish *Nature* **302** 61–2

Mangalam S, Syst T and Williamsburg V 2004 Real-time extraction of hydrodynamic flow characteristics using surface signatures *IEEE J. Ocean. Eng.* **29** 622–30

Mittal R, Dong H, Bozkurttas M, Lauder G V and Madden P 2006 Locomotion with flexible propulsors: II. Computational modeling of pectoral fin swimming in sunfish *Bioinsp. Biomim.* **1** S35–41

Ono R 1982 Proprioceptive endings in the myotomes of the pickeral (*Teleostei: Esocidae*) *J. Fish Biol.* **21** 525–35

Oppenheim A V, Schafer R W and Buck J R 1999 *Discrete-Time Signal Processing* 2nd edn (Upper Saddle River, NJ: Prentice-Hall) pp 474–8

Phelan C T, MacDonald R J and Tangorra J L 2009 Artificial muscle actuators in biorobotic fish fins *EMBC 2009: Ann. Int. Conf. IEEE (3–6 September 2009)* (Engineering in Medicine and Biology Society) pp 6822–5

Seo K, Chung S and Slotine J 2010 CPG-based control of a turtle-like underwater vehicle *Auton. Robots* **28** 247–69

Standen E and Lauder G 2005 Dorsal and anal fin function in bluegill sunfish *Lepomis macrochirus*: three-dimensional kinematics during propulsion and maneuvering *J. Exp. Biol.* **208** 2753–63

Tangorra J, Davidson S, Hunter I, Madden P, Lauder G, Dong H, Bozkurttas M and Mittal R 2007 The development of a biologically inspired propulsor for unmanned underwater vehicles *IEEE J. Ocean. Eng.* **32** 533–50

Tangorra J L, Esposito C J and Lauder G V 2009 Biorobotic fins for investigations of fish locomotion *IROS 2009: Intelligent Robots and Systems 2009, IEEE/RSJ Int. Conf.* (10–15 October 2009) pp 2120–5

Tangorra J, Lauder G, Hunter I, Mittal R, Madden P and Bozkurttas M 2010 The effect of fin ray flexural rigidity on the propulsive forces generated by a biorobotic pectoral fin *J. Exp. Biol.* submitted

Tangorra J L, Lauder G V, Madden P G, Mittal R, Bozkurttas M and Hunter I W 2008 A biorobotic flapping fin for propulsion and maneuvering *ICRA 2008: Robotics and Automation 2008 IEEE Int. Conf.* (19–23 May 2008) pp 700–5

Thorsen D and Hale M 2007 Neural development of the zebrafish (*Danio rerio*) pectoral fin *J. Comp. Neurol.* **504** 168–84

Webb J, Fay R and Popper A 2008 *Fish Bioacoustics* (New York: Springer)